

## X-ray diffraction mapping of strain fields and chemical composition of SiGe:Si(001) quantum dot molecules

M. S. Leite,<sup>1,2</sup> J. L. Gray,<sup>3</sup> R. Hull,<sup>3</sup> J. A. Floro,<sup>4</sup> R. Magalhães-Paniago,<sup>1,5</sup> and G. Medeiros-Ribeiro<sup>1</sup>

<sup>1</sup>Laboratório Nacional de Luz Síncrotron, Caixa Postal 6192, CEP-13084-971 Campinas, São Paulo, Brazil

<sup>2</sup>Instituto de Física Gleb Wataghin, UNICAMP, 13083-970 Campinas Brazil

<sup>3</sup>Department of Materials Science and Engineering, University of Virginia, Charlottesville, Virginia 22903, USA

<sup>4</sup>Sandia National Laboratories, Livermore, California 94550, USA

<sup>5</sup>Departamento de Física, UFMG, Belo Horizonte 30123-970, Brazil

(Received 5 November 2005; published 31 March 2006)

A variety of surface morphologies can be formed by controlling kinetic parameters during heteroepitaxial film growth. The system reported is a Si<sub>0.7</sub>Ge<sub>0.3</sub> film grown by molecular beam epitaxy at 550 °C and a 1 Å/s deposition rate, producing quantum dot molecule (QDM) structures. These nanostructures are very uniform in size and shape, allowing strain mapping and chemical composition evaluation by means of anomalous x-ray diffraction in a grazing incidence geometry. Tensile and compressed regions coexist inside QDMs, in accordance with the finite-element calculations of lattice relaxation. The Ge content was found to vary significantly within the structures, and to be quite different from the nominal composition.

DOI: 10.1103/PhysRevB.73.121308

PACS number(s): 68.55.Ac, 68.35.Gy, 61.10.Nz, 81.16.Rf

SiGe:Si(001) has been considered as a model system for strained epitaxial growth. This assumption stems from the fact that only two elements are involved, which are completely miscible in one another. Depending on kinetic and thermodynamic factors, such as temperature, deposition rate, and film composition, a large number of interesting structures can be created. For instance, pits<sup>1,2</sup> as well as hut clusters,<sup>3</sup> with very well-defined (105) facets can be formed, for growth conditions that are not too dissimilar. At higher temperatures, higher indexed faceted clusters appear, including domes<sup>4–7</sup> and dislocated domes.<sup>8,9</sup> The relative contributions of thermodynamics and kinetics processes to the formation of these systems are nevertheless somewhat hard to distinguish, given the numbers of parameters one has in heteroepitaxial growth.

As shown recently, in a regime of relatively low growth temperatures (about 550 °C),<sup>10,11</sup> the surface morphology can be controlled by varying the growth rate and film thickness. The preferred formation of pyramidal pits is followed by the nucleation of (105)-faceted elongated islands surrounding the pit, leading to quantum dot molecules (QDMs). This cooperative nucleation process<sup>12</sup> takes place at a growth rate of 0.9 Å/s for 50–300 Å thick films. Enlargement of QDMs is suppressed at a particular size, defined by the kinetics of adatoms attachment and diffusion, leading to a narrow size distribution.<sup>13</sup> For a thorough understanding of the formation of these structures, knowledge of their strain and compositional fields is needed. The evaluation of the chemical composition and strain profile of SiGe nanostructures has been demonstrated previously by the grazing incidence anomalous x-ray diffraction (GIXRD).<sup>14–16</sup> Recently, Krause *et al.* have also used this technique to evaluate shape, strain, and ordering in InAs QDMs.<sup>17</sup> The goal of this paper is the investigation of compositional inhomogeneities in QDMs using GIXRD, which will help to elucidate the mechanisms of QDM formation.

Two samples with nominal composition of Si<sub>0.7</sub>Ge<sub>0.3</sub> and different film thicknesses were grown by molecular beam epitaxy (MBE) in a custom-built double chamber system

with a base pressure of less than  $1 \times 10^{-10}$  Torr.<sup>10</sup> A 1000 Å Si buffer layer was initially grown on a nominally flat Si(001) at 750 °C. The SiGe films were grown at 550 °C and a deposition rate of approximately 1 Å/s. Atomic force microscopy (AFM) showed that the surface of the first sample was comprised of only pits, formed after the deposition of a 50 Å thick film, corresponding to the onset of the QDM formation (pit sample). The second sample was comprised of QDMs formed after 300 Å: fourfold symmetric groupings of 105-faceted islands surrounding a 105-faceted central pit that extends partway down into the thick, and otherwise planar, SiGe wetting layer (QDM sample). AFM analysis revealed very uniform size and shape distributions for the QDMs, with islands approximately  $3.0 \pm 0.3$  nm in height above the planar film surface, and  $150 \pm 7$  nm in length with  $58 \pm 6$  nm in thick walls. The depth of the pyramidal pits is about 8 nm below the surface. An AFM image of one QDM and one pit are shown in the inset of Fig. 1. The corresponding line scans are shown along the [010] direction. The QDM line scan also shows the (105)-facet bounded ridge (SiGe islands), as well as the presence of a moat around the QDM.

GIXRD measurements using different x-ray energies to exploit anomalous diffraction were the primary tool for the investigation of composition and strain mapping.<sup>14,16</sup> The GIXRD experiments were performed at the XRD1 x-ray diffraction beam line of the Brazilian National Synchrotron Light Source. The use of grazing incidence geometry and synchrotron radiation were essential to maximize the island-substrate intensity ratio. Two types of measurements with the same experimental setup were performed: radial and angular scans. Radial scans are regular  $\theta$ - $2\theta$  measurements, which produce an in-plane lattice spacing histogram given by the scattered intensity as a function of the Bragg condition ( $a' = \lambda \sqrt{h^2 + k^2 + l^2} / [2 \sin(2\theta/2)]$ , where  $hkl$  are the Miller indices of the nearest Bragg reflection). The angular ( $\omega$ ) scan is done at a fixed diffraction angle ( $2\theta$ ) that determines the size of the scattering region for a constant lattice spacing. In re-

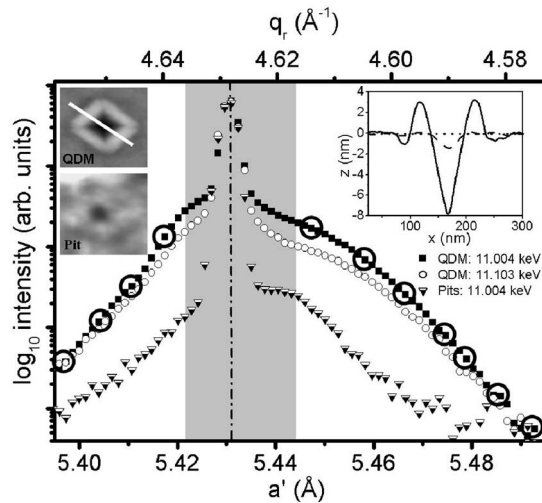


FIG. 1. Anomalous x-ray radial scans of the QDM sample at 11.004 and 11.103 keV and the pit sample at 11.004 keV, showing a significant variation in the scattered intensities. The difference is associated with the Ge content within QDMs. The intensity in the  $\log_{10}$  scale is shown as a function of the lattice spacing  $a'$  (Å). For  $a'$  larger than Si more Ge is expected. The peak around 5.431 Å corresponds to the substrate scattering. The open circles mark the  $a'$  corresponding to angular scans used in the strain profile analysis. Insets: AFM images of  $250 \times 250$  nm<sup>2</sup> showing one QDM and one pit. The corresponding line scans (dashed line—pit, solid line—QDM) are along the [010] direction.

reciprocal space, the momentum transfer vectors associated with radial [ $q_r = (4\pi/\lambda)\sin(2\theta/2)$ ] and angular [ $q_a = (4\pi/\lambda)\sin(\theta - 2\theta/2)$ ]<sup>16</sup> scans are perpendicular. The measurements were all performed near the (400) reflection, i.e.,  $h=4$  and  $k=l=0$ , which represented the best condition for the experimental configuration used taking into account both signal intensity and contrast between Si and Ge.<sup>14</sup>

Figure 1 shows radial scans at the same energy— $E_1 = 11.004$  keV—for the pit (triangles) and the QDM (closed squares) samples. The x-ray spot on the sample covered a macroscopic region of the surface, hence, producing statistically significant data. The scattered intensity in the  $\log_{10}$  base is shown as a function of the in-plane lattice spacing  $a'$  (Å), and it is proportional to the volume of the material at that particular Bragg condition. The peak around 5.431 Å ( $a_{Si}$ ) corresponds to the substrate scattering (in gray in the graph). There are two distinct regions in the graph: one with lattice spacing smaller than the Si lattice parameter and another with  $a' > a_{Si}$ . FEC<sup>13</sup> indicates that material with  $a' < a_{Si}$  correspond to regions near the pit cusp, and  $a' > a_{Si}$  are from regions higher than the planar wetting layer surface. Even for the pit sample there is some material with  $a' > a_{Si}$ . It is likely that it corresponds to the pit rim, given the fact that there are no islands. This region could act as a nucleation site for the island and thus for QDMs development. For thicker layers, this region preferentially attracts material, thus forming QDMs.

It is of primary importance to determine whether QDMs remain at the nominal composition of the film, or if there is any inhomogeneous compositional redistribution during growth,<sup>20</sup> as has been previously observed during SiGe quan-

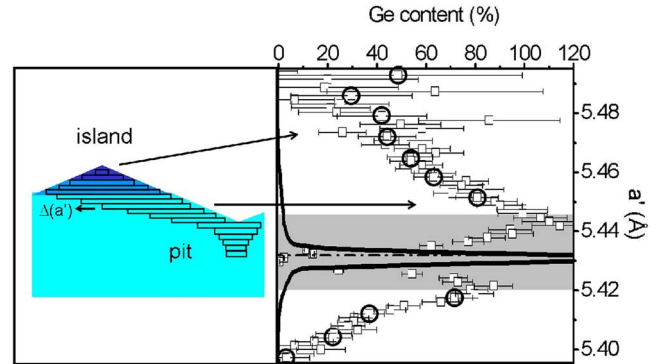


FIG. 2. (Color online) Cross-section representation of the QDM and SiGe films.  $\Delta(a')$  is the thickness of each scattering object contributing to the x-ray signal. Graph of the Ge content as a function of the lattice spacing  $a'$  (Å). It is possible to associate the Ge concentration with different QDM regions, shown in the two-dimensional representation. The solid line corresponds to a radial scan on a linear scale, showing the scattered intensity of the Si substrate and the wetting layer. The open circles mark the  $a'$  corresponding to angular scans used in the strain profile analysis.

tum dot formation.<sup>18</sup> By using two different x-ray energies, one of which ( $E_2 = 11.103$  keV) is very close to the Ge  $K$ -absorption edge, one can obtain chemical sensitivity. This occurs because the complex atomic scattering factor  $f_{Ge_2}$  changes from  $E_1$  ( $f_{Ge_1} = 16.0 + 0.5i$ ,  $f_{Ge_2} = 11.1 + 2.0i$ ) near the absorption edge. However,  $f_{Si}$  is constant at  $7.8 + 0.2i$  for the whole range. The difference in the Ge atomic factor induces a significant variation in the scattered intensity, and the ratio varies as:<sup>15</sup>

$$\frac{I_1}{I_2} = \left| \frac{C_{Ge}f_{Ge_1} + C_{Si}f_{Si}}{C_{Ge}f_{Ge_2} + C_{Si}f_{Si}} \right|^2, \quad (1)$$

where  $I_1$  and  $I_2$  are the scattered intensity at  $E_1$  and  $E_2$ , respectively;  $C_{Ge}$  is the Ge content and  $C_{Si}$  is the Si content. Figure 1 shows the scattered intensities; the ratio is clearly observed to vary, which unambiguously demonstrates that the QDM composition is inhomogeneous. Knowing that  $C_{Si} + C_{Ge} = 1$ , the Ge concentration can be inferred from

$$C_{Ge} \cong \left[ 1 + \frac{f_{Ge_2}\sqrt{I_1} - f_{Ge_1}\sqrt{I_2}}{f_{Si}(\sqrt{I_2} - \sqrt{I_1})} \right]^{-1}. \quad (2)$$

Using Eq. (2),  $C_{Ge}$  (%) of the QDM sample was determined quantitatively as a function of lattice spacing  $a'$  (Å). The results of the direct composition analysis of the scattering data are shown in Fig. 2. The Ge concentration strongly deviates from the nominal composition of the film, with the enrichment reaching nearly 100% Ge, indicating significant atomic redistribution during growth. While Fig. 2 appears to show two enrichment peaks, one at  $a' = 5.442$  Å and one at 5.420 Å, the more likely interpretation of the figure is that there is a broad “band” of Ge enrichment, centered near the Si lattice parameter, that encompasses portions of the QDM that are both slightly relaxed and regions that are slightly overcompressed. Note that in between these two peaks it is impossible to separate the substrate signal from the wetting

layer one, as well as any contribution from material within the QDM at this Bragg condition. This is due to the fact that the volume of the two regions differs by several orders of magnitude (see the solid line in the graph of Fig. 2, corresponding to a radial scan in linear scale). As a consequence, the region in gray in the graph does not provide reliable information, and thus is omitted in the calculation of composition and, hence, the data falling within this region will not be used in all the subsequent analysis.

While Ge enrichment in partly relaxed regions of the QDM is easy to understand, the enrichment in regions that are overcompressed is more problematic, and may arise for purely kinetic reasons. Nonetheless, the data are clear on this. It is important to emphasize that the data of Fig. 2 do not depend on any model for the shape or strain field of a QDM—it is sufficient to know the atomic scattering factor, which is well characterized.

The Ge enrichment decreases for increasing lattice spacing, which correlates with increasing island heights and is very close to the nominal composition (about 30%) at the top. Using Vegard's law, one can estimate the lattice spacing variation in different regions of the film and calculate the local strain  $\varepsilon$ . At the top of the island,  $x \cong 0.3$ ,  $a(x) = a'$  is equal to 5.49 Å and the strain is close to zero. By calculating the strain and the evaluated composition for each Bragg condition, the material was found to be compressed for  $a' < a_{Si}$  and partially relaxed for  $a' > a_{Si}$  (negative strain). In order to locate the regions of high Ge content within the QDM, the structure was modeled as a stack of equal-lattice spacing regions (see the representation in Fig. 2),<sup>16</sup> corresponding to different Bragg conditions displayed by the radial scan (Fig. 1).

Besides the radial scans, which provide the distribution of lattice spacings within the samples, angular scans can be carried out to ascertain the approximate mean size of the scattering region associated with each lattice spacing. Angular scans were performed for selected lattice spacings. As discussed previously, only the circled data points in Figs. 1 and 2 are not affected by the substrate signal. Figure 3(a) shows examples of three of these angular scans performed on the QDM sample. The scattered intensity of a square object of size  $L$  for this scattering geometry can be approximated as a Gaussian function [solid lines in Fig. 3(a)]. The object size for each  $a'$  is determined by the full-width-half-maximum [FWHM— $\Delta q_{a'}$ ] of the Gaussian curves, estimated by the following equation,

$$L_{a'} = \frac{2\pi}{\Delta q_{a'}}. \quad (3)$$

Figure 3(b) shows the  $L_{a'}$  dependence on  $a'$ . Both the overcompressed region (near the cusp of the pit) and the most relaxed region (at the top of the islands) have a limited spatial extent, as expected. The islands at the perimeter of the pit forming the QDMs are elongated, thus distorting the in-plane lattice spacings according to the length of the islands. In one direction, the smaller and larger sides ( $L_s$  and  $L_l$  in the representation of Fig. 3) of the QDMs have the same  $a'$  at different heights. Since more relaxation takes place along the

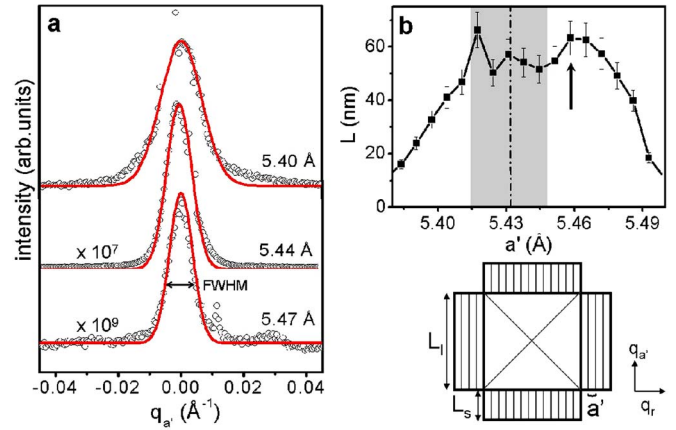


FIG. 3. (Color online) (a) Angular scans of the QDM sample measured at 11.004 keV. Each curve is associated with a different lattice spacing (the values are indicated). The measurements were performed near the (400) reflection. The solid lines correspond to Gaussian approximations. (b) Graphic of the size of the scattering object  $L$  (nm) as a function of the lattice spacing  $a'$  (Å). Each point is determined through the FWHM of the Gaussian fits. Below: top view representation of a single QDM showing the smaller and larger sides— $L_l$  and  $L_s$ —of the islands, which corresponds to different heights, besides the same lattice spacing.

short direction, for the same  $a'$ ,  $h[L_s(a')] < h[L_l(a')]$ . Thus, contribution of the scattering of  $L_l$  at the Bragg condition is minimal owing to a much smaller volume. This fact allows a direct correlation of each angular scan with  $L_s$ . The largest  $L_s$  is about 60 nm, in agreement with the short width of the island base, as measured by AFM.

The coupling of the lateral size of each scattering volume to some mean height within the QDM structure permits the construction of a vertical composition profile. For simple quantum dots, this can be done fairly straightforwardly. However, for the much more complex QDM structure, the assignment of a height scale is difficult, and must be taken as approximate. Nonetheless, the exercise is worthwhile in order to evaluate both the veracity of the method, and how to proceed with future analysis. Knowing the object size  $L_{a'}$  for each  $a'$  and the fact that the structures are (105)-facet bounded, a relationship between the height  $h$  (nm) of the object and its lattice spacing can be established, according to the following expression,

$$h(a) = \sum_{a_0}^a \Delta(a') + C = k \sum_{a_0}^a \frac{I_{a'}}{L_{a'}^2} + C. \quad (4)$$

Summing the thickness of each object  $\Delta(a')$  associated with a different  $a'$  from the mostly compressed region  $a_0$  to the actual lattice parameter  $a$ , one can evaluate the compositional and strain profiles from the top of the QDM into the strained regions of the substrate. The expression is derived from the relationship between scattered intensity as a function of scattering volume,  $I(a') = kL^2(a')\Delta(a')$ , where  $k$  is a constant that takes into account the object anisotropy, the scattering factors, and the detector efficiency.  $k$  is determined upon direct comparison of the inferred  $h(L)$  relationship and

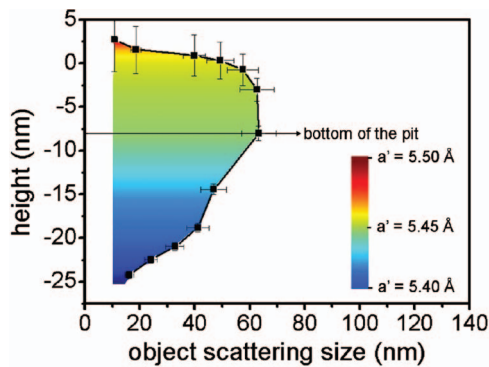


FIG. 4. (Color) Relation between the size of each scattering object size (nm) determined by anomalous GIXRD angular scans and the QDM height (nm). The color scale is associated with the lattice spacing variation in the film.

the AFM line profile. The constant  $C$  defines the film surface [see the arrow in Fig. 3(b)]. The result of applying Eq. (4) to the data produces the relationship between the size of each object to its depth with respect to the sample surface. Comparing this result to an AFM line scan for a statistically representative QDM, one can estimate how  $a'$  changes across the whole structure (shown in Fig. 4). The local lattice spacing variation, compared with island height  $h$ , gives a strain  $\epsilon$  map of the SiGe film [Fig. 5(a)]. The island top corresponds to the more relaxed region (in blue), whereas the pit region is overcompressed ( $\epsilon = -3\%$  at the bottom of the pit, in dark red), in rough accord with FECs performed with similar morphologies.<sup>13</sup> This represents a semiquantitative picture of local strain within QDMs.

In Fig. 5(b), the Ge content (%) is shown as a function of QDM  $h$  (nm), deduced from the anomalous GIXRD measurements. There is a Ge enrichment of the bounding islands close to the base and toward the pit cusp; whereas, at the top, the composition is closer to the nominal value. As pointed out recently,<sup>19</sup> the understanding of QDM formation is incomplete. In particular, Ref. 19 showed that the simple picture wherein the bounding islands are entirely formed from the atoms leaving the central pit is insufficient—the islands contain nearly three times more volume than is missing from the pit, and therefore significant atom incorporation from the surrounding wetting layer must also occur. It is important to recall that the composition profiles measured represent a snapshot of the total QDM evolutionary process. It could be that some of the Ge enrichment was established at an earlier

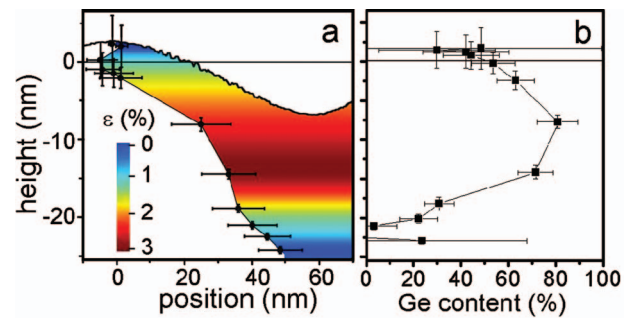


FIG. 5. (Color) (a) Atomic force microscopy line scan of one QDM showing the local strain variation (color scale). There is a coexistence of compressive and relaxed materials. (b) Ge content (%) as a function of QDM height (nm) composed by anomalous XRD measurements.

stage of QDM formation. Tersoff<sup>20</sup> pointed out that pits can relax strained surfaces more efficiently than pyramids. It is thus reasonable to expect the regions in and around the *original* pits to be richer in Ge. As the QDM grows, this high Ge concentration may get locked into a meta-stable configuration that we subsequently measure. Of course, the x-ray data analysis may be oversimplistic given the complex geometry; however, the essential phenomena involved in QDM formation can be captured in the analysis presented.

In this communication, compositional and strain variation in SiGe QDM nanostructures were evaluated using anomalous GIXRD. It was found that Ge concentration significantly varies about the nominal composition of 30%, which had copious Ge adatom redistribution during film growth. In particular, there are regions within the four quantum dots comprising a QDM where the composition reaches almost 100% Ge. The existence of buried Ge-rich dots will be important for carrier confinement in device applications such as quantum cellular automata.<sup>13</sup> The anomalous scattering data showed the existence of an unexpected Ge-rich region immediately below the QDM pit, which must arise from the kinetically limited growth process that forms QDMs.

The authors M.S.L., R.M.P., and G.M.R. acknowledge FAPESP (Contract No. 03/09374-9) and CNPq for financial support. Work at Sandia was supported by the DOE Office of Basic Energy Sciences. Sandia is a multiprogram laboratory of the U.S. Department of Energy operated by Sandia Corporation, a Lockheed Martin Company, under Contract No. DE-AC04-94AL85000.

<sup>1</sup>K. M. Chen *et al.*, Appl. Phys. Lett. **66**, 34 (1995).

<sup>2</sup>I. Goldfarb *et al.* Phys. Rev. Lett. **78**, 3959 (1997).

<sup>3</sup>Y.-W. Mo *et al.*, Phys. Rev. Lett. **65**, 1020 (1990).

<sup>4</sup>M. Tomitori *et al.*, Appl. Surf. Sci. **76–77**, 322 (1994).

<sup>5</sup>J. A. Floro *et al.*, Phys. Rev. Lett. **80**, 4717 (1998).

<sup>6</sup>F. M. Ross *et al.*, Phys. Rev. Lett. **80**, 984 (1998).

<sup>7</sup>G. Medeiros-Ribeiro *et al.*, Science **279**, 353 (1998).

<sup>8</sup>S. A. Chaparro *et al.*, Phys. Rev. Lett. **83**, 1199 (1999).

<sup>9</sup>U. Denker *et al.* Appl. Phys. Lett. **772**, 599 (2005).

<sup>10</sup>J. L. Gray *et al.*, Appl. Phys. Lett. **81**, 2445 (2002).

<sup>11</sup>J. T. E. Vandervelde *et al.*, Appl. Phys. Lett. **83**, 2505 (2003).

<sup>12</sup>D. E. Jesson *et al.*, Phys. Rev. Lett. **77**, 1330 (1996).

<sup>13</sup>J. L. Gray *et al.*, Phys. Rev. Lett. **92**, 135504 (2004).

<sup>14</sup>T. U. Schüllli *et al.*, Phys. Rev. Lett. **90**, 066105 (2003).

<sup>15</sup>A. Malachias *et al.* Phys. Rev. Lett. **91**, 176101 (2003).

<sup>16</sup>R. Magalhães-Paniago *et al.*, Phys. Rev. B **66**, 245312 (2002).

<sup>17</sup>B. Krause *et al.*, Phys. Rev. B **72**, 085339 (2005).

<sup>18</sup>Y. Zhang *et al.*, J. Appl. Phys. **90**, 4748 (2001).

<sup>19</sup>J. L. Gray *et al.*, Phys. Rev. B **72**, 155323 (2005).

<sup>20</sup>J. Tersoff, Phys. Rev. Lett. **81**, 3183 (1998).